Supplementary Figures

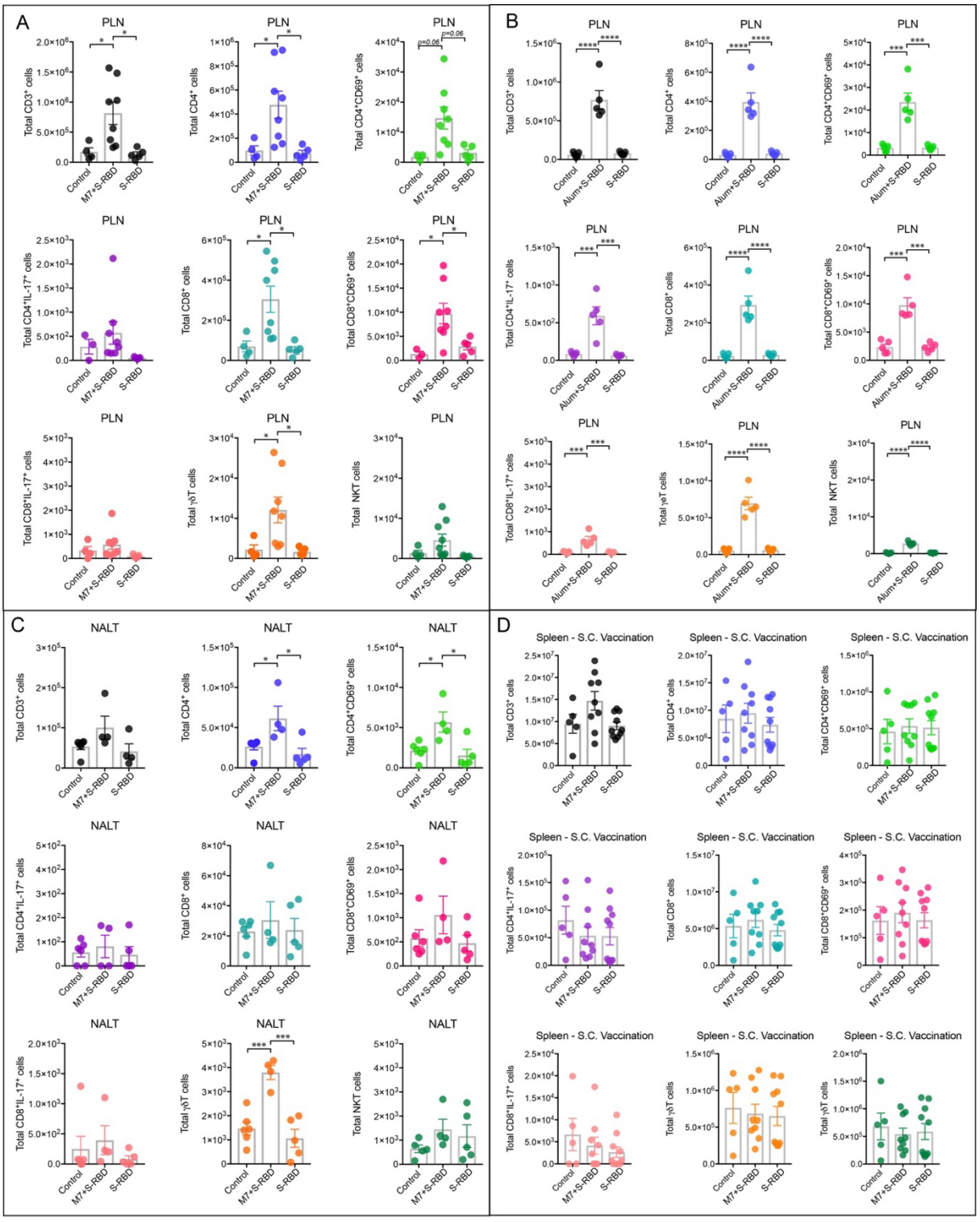

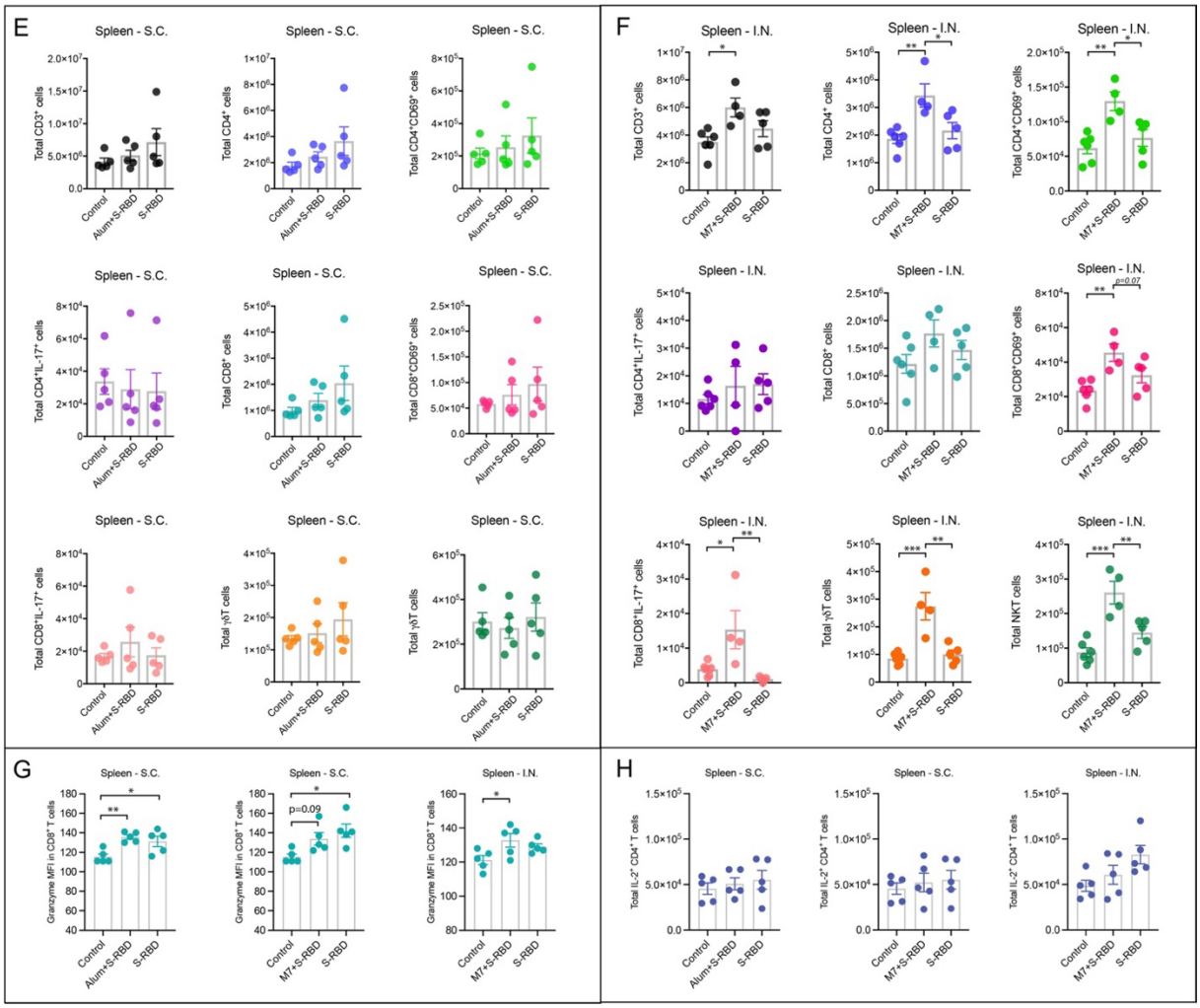

Figure S1: Enhanced systemic T cell activation following mucosal vaccination
(**A-C**) Plots showing the total numbers of various subsets of T cells day 5 following vaccination in the draining lymphoid tissue [either NALT or popliteal LN (PLN)] for the following groups: (**A**) M7+S-RBD S.C. (**B**) Alum+S-RBD (**C**) M7+S-RBD I.N. (**D-F**) Plots showing the total numbers of various subsets of T cells on day 5 following vaccination in the spleen for the following groups: (**D**) M7+S-RBD S.C. (**E**) Alum+S-RBD, and (**F**) M7+S-RBD I.N. (**G**) Mean fluorescence intensity (MFI) of Granzyme B expression in splenic $CD8^+$ T cells. (**H**) Plots showing the total numbers of IL-2-expressing $CD4^+$ T cells in the spleen. Groups were compared by 1-way ANOVA with Holm-Sidak's posttest; *p<0.05; **p<0.01; ***p<0.001; ****p<0.0001. Corresponding cell frequencies are provided in **Table S3**.

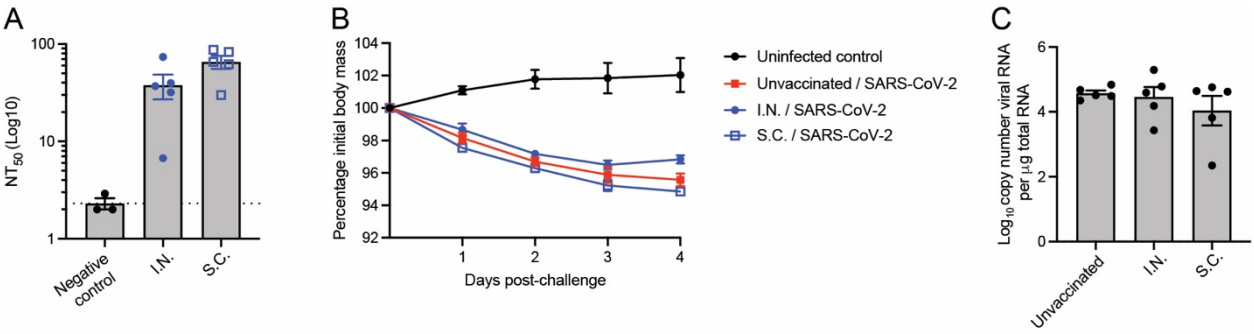

Figure S2: Serological, clinical and virological outcomes following vaccination in the hamster model

(**A**) Neutralizing antibodies were detected in all vaccinated hamsters, day 35 prior to challenge by plaque reduction neutralization test (PRNT). (**B**) Hamster weight was monitored following challenge and significantly declined in all SARS-CoV-2-challenged groups, by two-way ANOVA with Tukey's post-test, ****p<0.001. (**C**) No significant differences in viral genome quantification in the lungs were observed between groups day 4 post-infection by one-way ANOVA.

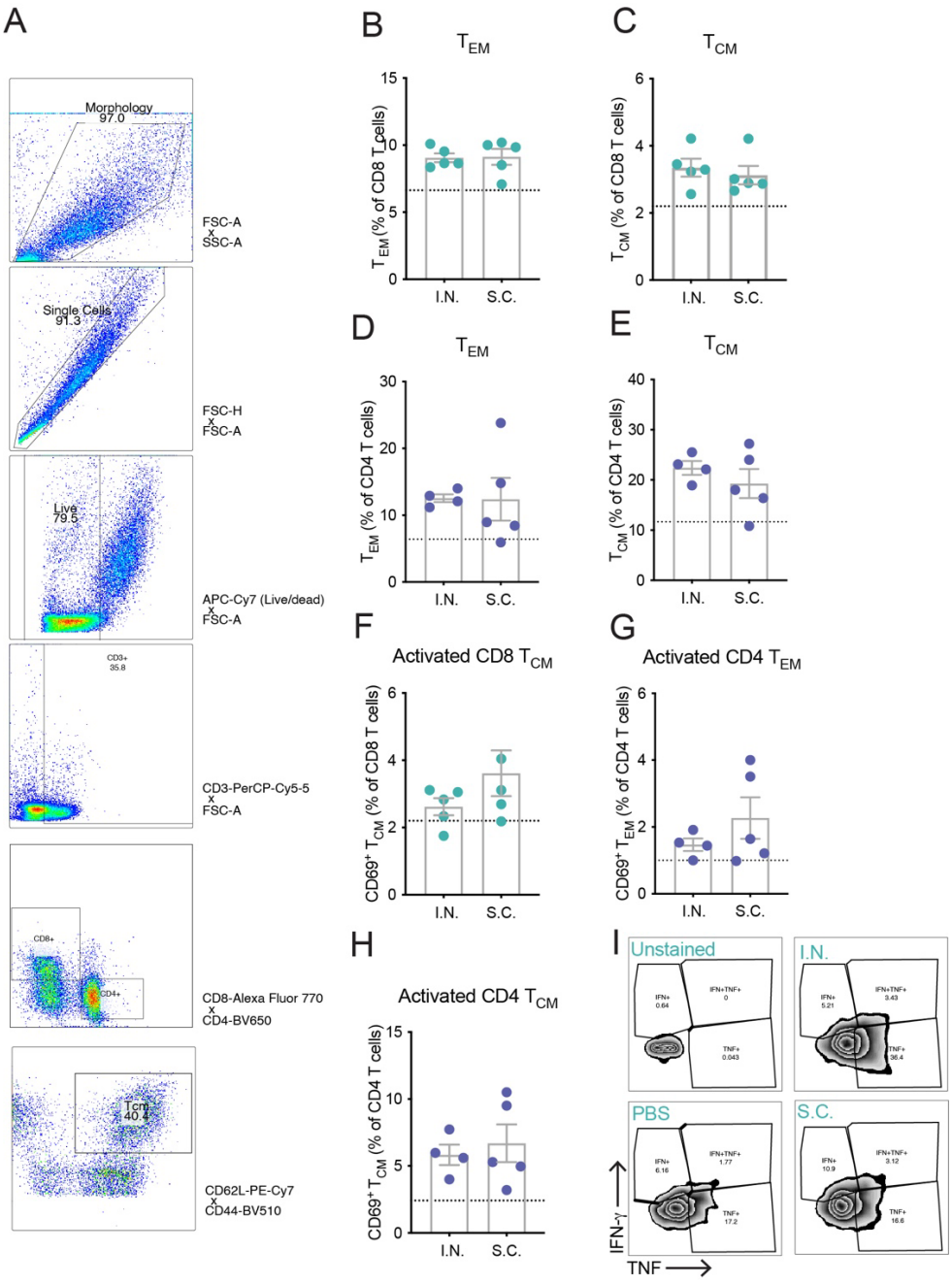

Figure S3: Activation of several T_{MEM} subsets by *ex vivo* antigen stimulation
(**A**) Gating strategy to identify memory T cell subsets in co-culture. Percentages of (**B-C**) CD8 memory and (**D-E**) CD4 memory subsets or (**F**) Activated CD8 T_{CM} or activated (**G-H**) memory CD4 T cells, following S-RBD stimulation. All groups in B-H were compared by Student's unpaired t-test and found to not differ significantly. (**I**) Representative plots showing intracellular staining of T_{MEM} cells for IFN-γ and TNF for unstained compensation controls (gated only with the morphology gate shown in panel A), and PBS, I.N. and S.C. groups.

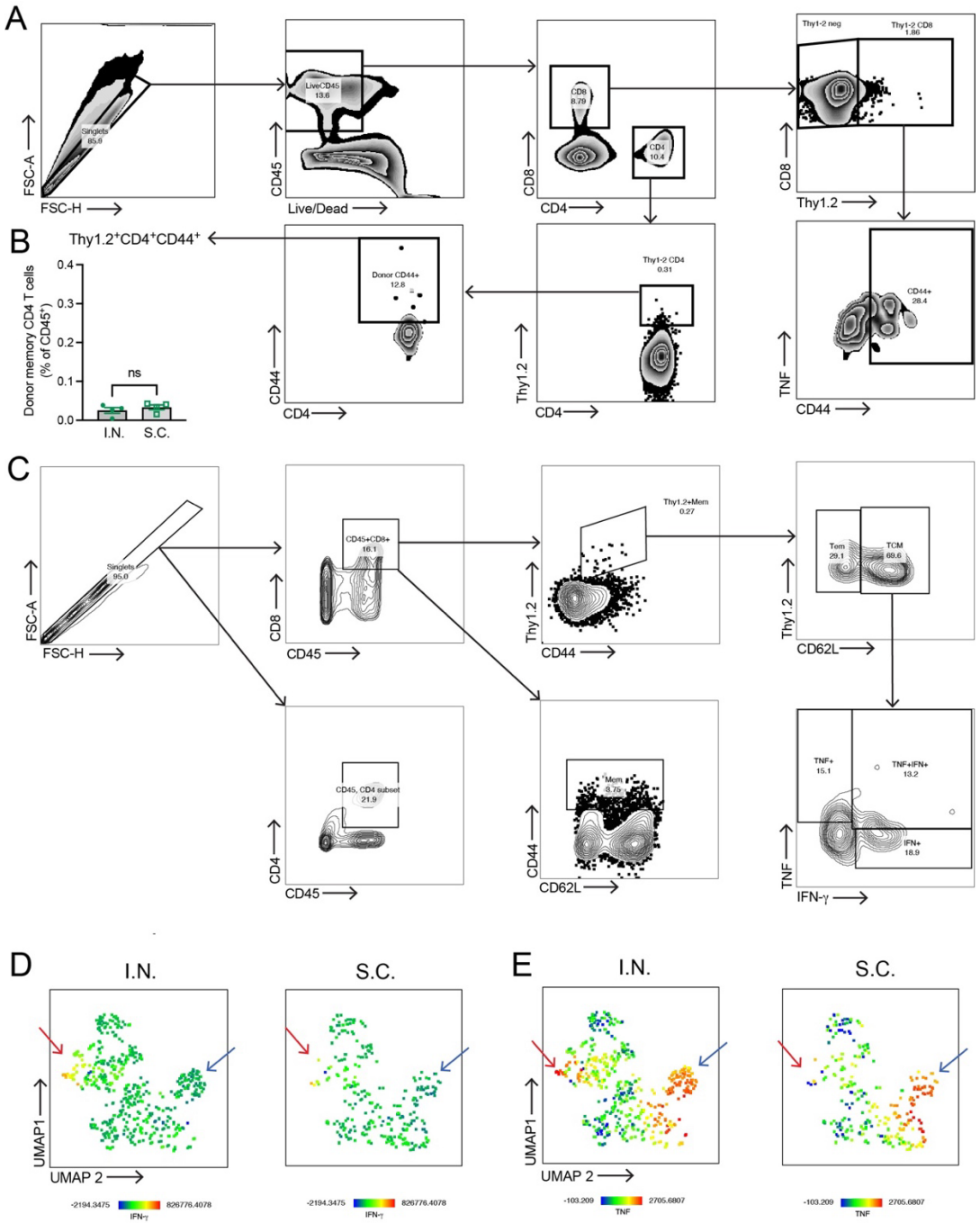

Figure S4. Identification and characterisation of donor T cell phenotypes following *in vivo* antigen challenge

(**A**) Flow cytometry gating strategies to identify donor Thy1.2^{+} T cell populations in the lungs (**B**) Donor Thy1.2^{+} CD4 T cells constituted a minor portion of hemopoietic cells in the lung following challenge and did not differ in frequency between I.N. or S.C. M7+S-RBD vaccinated groups.

(**C**) Flow cytometry gating strategies to identify donor Thy1.2^{+} T cell populations in the brachial LNs. (**D-E**) Heat maps depicting (**D**) IFN-γ and (**E**) TNF expression in T_{MEM} cells of the brachial LNs. Areas with cytokine expressing CD4 T cells are indicated with red arrows and areas with cytokine expressing CD8 T cells are indicated by blue arrows.

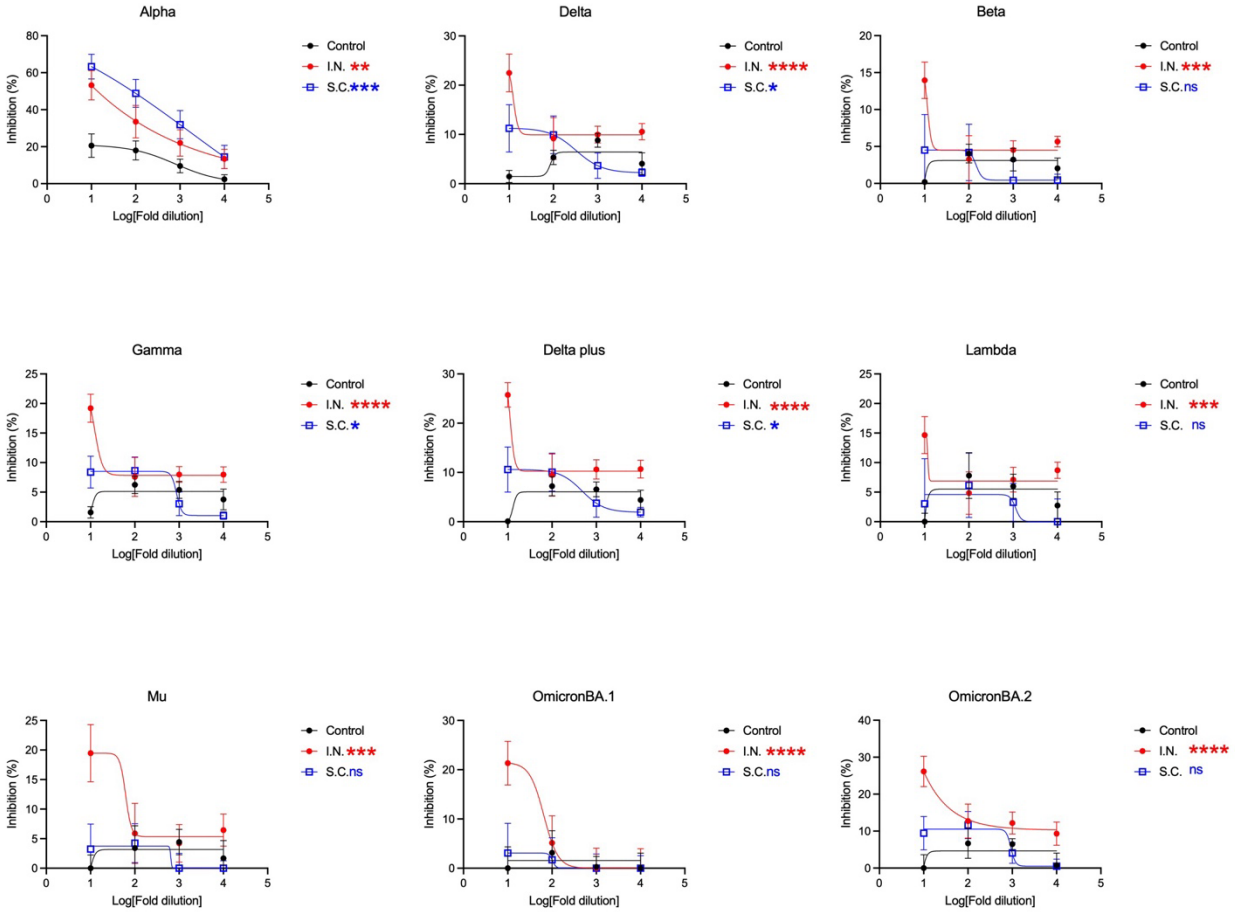

Figure S5. Improved serum cross-neutralization of SARS-CoV-2 variants following mucosal immunisation. Dose response curves showing the % inhibition against S-RBD from multiple SARS-CoV-2 variants by s-VNT assay. P-values were determined by 2-way ANOVA. *p<0.05, **p<0.01, ***p<0.001 ****p<0.0001 by two-way ANOVA.

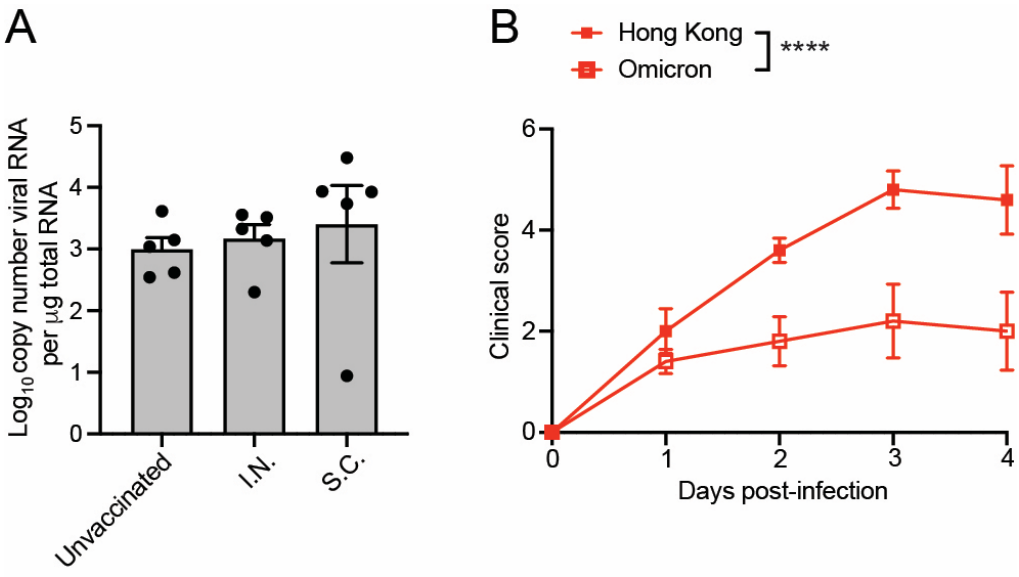

Figure S6: Infection burden and clinical scores in Omicron-challenged hamsters vaccinated with parental strain S-RBD.

(**A**) No significant differences in viral genome quantification were observed in lungs of Omicron challenged hamsters, by 1-way ANOVA. (**B**) Significantly reduced clinical scores for Omicron-infected hamsters compared to Hong Kong (parental strain)-infected hamsters by two-way ANOVA, $p<0.0001$.

Supplementary Tables

Table S1: Predicted mouse MHC-I-binding peptides in the RBD of S-protein

Peptide predictions for binding to the MHC-I molecules found in C57Bl/6 mice (H-2-Db, H-2-Dd, H-2-Kb and H-2-Kd) for the RBD domain of S-protein (Accession # QHD43416) were performed using TepiTool(1) and the top 2% of predicted binders based on percentile rank are presented.

Peptide start	Peptide end	Peptide	IEDB consensus percentile rank	Allele
126	134	KVGGNYNYL	0.09	H-2-Db
48	56	SVLYNSASF	0.1	H-2-Db
187	195	YQPYRVVVL	0.17	H-2-Db
47	56	YSVLYNSASF	0.17	H-2-Db
7	17	SIVRFPNITNL	0.17	H-2-Db
9	17	VRFPNITNL	0.25	H-2-Db
159	168	STPCNGVEGF	0.3	H-2-Db
64	72	VSPTKLNDL	0.33	H-2-Db
125	134	SKVGGNYNYL	0.37	H-2-Db
8	17	IVRFPNITNL	0.38	H-2-Db
179	187	FQPTNGVGY	0.58	H-2-Db
191	199	RVVVLSFEL	0.65	H-2-Db
192	200	VVVLSFELL	0.68	H-2-Db
90	100	RQIAPGQTGKI	0.69	H-2-Db
207	215	CGPKKSTNL	0.72	H-2-Db
115	123	VIAWNSNNL	0.78	H-2-Db
127	134	VGGNYNYL	1.1	H-2-Db
64	72	VSPTKLNDL	0.01	H-2-Dd
207	215	CGPKKSTNL	0.01	H-2-Dd
206	215	VCGPKKSTNL	0.02	H-2-Dd
187	195	YQPYRVVVL	0.04	H-2-Dd
205	215	TVCGPKKSTNL	0.05	H-2-Dd
185	195	VGYQPYRVVVL	0.07	H-2-Dd
92	100	IAPGQTGKI	0.13	H-2-Dd
208	215	GPKKSTNL	0.2	H-2-Dd
185	193	VGYQPYRVV	0.2	H-2-Dd
51	59	YNSASFSTF	0.25	H-2-Dd
9	17	VRFPNITNL	0.29	H-2-Dd
64	74	VSPTKLNDLCF	0.3	H-2-Dd
2	11	VQPTESIVRF	0.43	H-2-Dd
10	17	RFPNITNL	0.46	H-2-Dd
6	14	ESIVRFPNI	0.49	H-2-Dd
185	192	VGYQPYRV	0.51	H-2-Dd

62	72	YGVSPTKLNDL	0.58	H-2-Dd
129	137	GNYNYLYRL	0.01	H-2-Kb
7	14	SIVRFPNI	0.01	H-2-Kb
193	200	VVLSFELL	0.01	H-2-Kb
131	138	YNYLYRLF	0.03	H-2-Kb
185	192	VGYQPYRV	0.04	H-2-Kb
185	193	VGYQPYRVV	0.06	H-2-Kb
9	17	VRFPNITNL	0.07	H-2-Kb
116	123	IAWNSNNL	0.1	H-2-Kb
192	200	VVVLSFELL	0.14	H-2-Kb
24	32	FNATRFASV	0.15	H-2-Kb
49	56	VLYNSASF	0.2	H-2-Kb
192	199	VVVLSFEL	0.2	H-2-Kb
64	72	VSPTKLNDL	0.2	H-2-Kb
127	137	VGGNYNYLYRL	0.2	H-2-Kb
130	137	NYNYLYRL	0.21	H-2-Kb
136	143	RLFRKSNL	0.21	H-2-Kb
127	134	VGGNYNYL	0.25	H-2-Kb
186	194	GYQPYRVVV	0.05	H-2-Kd
61	69	CYGVSPTKL	0.08	H-2-Kd
32	40	VYAWNRKRI	0.11	H-2-Kd
176	185	SYGFQPTNGV	0.19	H-2-Kd
9	17	VRFPNITNL	0.26	H-2-Kd
77	84	VYADSFVI	0.26	H-2-Kd
186	195	GYQPYRVVVL	0.27	H-2-Kd
10	17	RFPNITNL	0.3	H-2-Kd
60	69	KCYGVSPTKL	0.44	H-2-Kd
59	69	FKCYGVSPTKL	0.52	H-2-Kd
187	195	YQPYRVVVL	0.56	H-2-Kd
81	89	SFVIRGDEV	0.61	H-2-Kd
50	59	LYNSASFSTF	0.68	H-2-Kd
186	193	GYQPYRVV	0.7	H-2-Kd
185	194	VGYQPYRVVV	0.74	H-2-Kd
154	162	IYQAGSTPC	0.78	H-2-Kd
31	40	SVYAWNRKRI	0.86	H-2-Kd

Table S2: Predicted mouse MHC-II-binding peptides in the RBD of S-protein

Peptide predictions for binding to the MHC-II molecule found in C57Bl/6 mice (H2-IAb) were performed using TepiTool(1).

Peptide start	Peptide end	Peptide sequence	Consensus percentile rank	Allele
194	208	VLSFELLHAPATVCG	2.9	H2-IAb
151	165	STEIYQAGSTPCNGV	3.7	H2-IAb
45	59	ADYSVLYNSASFSTF	5.5	H2-IAb
56	70	FSTFKCYGVSPTKLN	6.45	H2-IAb
27	41	TRFASVYAWNRKRIS	7.45	H2-IAb
173	187	PLQSYGFQPTNGVGY	7.55	H2-IAb

Table S3: Cell frequencies corresponding to Figure 1.

Table values are provided as mean ± SD and were compared by 2-way ANOVA with Tukey's posttest. *p<0.05; **p<0.01; ****p<0.0001. Nonsignificant p-values below 0.1 are provided.

	Vaccine composition			
	Control	**Adjuvant+S-RBD**	**S-RBD**	**p-value**
Alum S.C. PLN				
CD4 (% of $CD3^+$)	51.6 ± 0.5	48.9 ± 3.1	50.9 ± 2.9	
$CD4^+CD69^+$ (% of $CD3^+$)	6.0 ± 1.0	11.1 ± 2.3	8.9 ± 9.0	*
$CD8^+$ (% of $CD3^+$)	38.0 ± 1.1	37.6 ± 2.2	37.4 ± 1.4	
$CD8^+CD69^+$ (% of $CD3^+$)	3.4 ± 0.6	10.6 ± 2.5	8.3 ± 2.7	*
$CD4^+IL\text{-}17^+$ (% of $CD4^+$)	0.15 ± 0.04	0.34 ± 0.19	0.17 ± 0.05	
$CD8^+IL\text{-}17^+$ (% of $CD8^+$)	0.22 ± 0.02	0.43 ± 0.11	0.31 ± 0.08	
gdT cell (% of $CD3^+$)	0.92 ± 0.07	0.80 ± 0.079	0.76 ± 0.11	
NKT cell (% of $CD3^+$)	0.38 ± 0.069	0.27 ± 0.066	0.25 ± 0.07	
Alum S.C. Spleen				
CD4 (% of $CD3^+$)	48.2 ± 3.6	42.0 ± 2.2	50.6 ± 4.2	****
$CD4^+CD69^+$ (% of $CD3^+$)	10.0 ± 3.1	12.3 ± 1.5	9.0 ± 2.4	*
$CD8^+$ (% of $CD3^+$)	26.8 ± 2.6	23.9 ± 1.2	27.6 ± 2.3	*
$CD8^+CD69^+$ (% of $CD3^+$)	5.3 ± 1.4	6.1 ± 1.5	4.8 ± 1.3	
$CD4^+IL\text{-}17^+$ (% of $CD4^+$)	1.08 ± 0.68	1.85 ± 0.46	0.75 ± 0.37	
$CD8^+IL\text{-}17^+$ (% of $CD8^+$)	1.68 ± 0.7	1.79 ± 0.58	0.93 ± 0.35	
gdT cell (% of $CD3^+$)	2.94 ± 0.32	3.34 ± 0.44	2.78 ± 0.35	
NKT cell (% of $CD3^+$)	5.42 ± 1.23	7.31 ± 0.99	4.94 ± 1.52	
M7 S.C. PLN				
CD4 (% of $CD3^+$)	52.2 ± 4.8	58.4 ± 0.6	51.1 ± 2.5	****
$CD4^+CD69^+$ (% of $CD3^+$)	3.0 ± 0.3	3.4 ± 0.5	2.5 ± 0.3	
$CD8^+$ (% of $CD3^+$)	43.1 ± 4.2	36.9 ± 0.6	43.9 ± 2.6	****
$CD8^+CD69^+$ (% of $CD3^+$)	1.8 ± 0.6	1.3 ± 0.2	1.5 ± 0.3	
$CD4^+IL\text{-}17^+$ (% of $CD4^+$)	0.14 ± 0.06	0.13 ± 0.04	0.13 ± 0.05	
$CD8^+IL\text{-}17^+$ (% of $CD8^+$)	0.16 ±0.1	0.07 ± 0.3	0.14 ± 0.09	
gdT cell (% of $CD3^+$)	1.27 ± 0.11	1.29 ± 0.19	1.35 ± 0.20	
NKT cell (% of $CD3^+$)	0.16 ± 0.05	0.18 ± 0.03	0.26 ± 0.12	
M7 S.C. Spleen				
CD4 (% of $CD3^+$)	53.1 ± 0.8	56.7 ± 1.4	53.1 ± 2.9	**
$CD4^+CD69^+$ (% of $CD3^+$)	2.90 ± 0.63	2.94 ± 0.61	3.59 ± 0.67	
$CD8^+$ (% of $CD3^+$)	35.5 ± 1.0	31.8 ± 2.8	32.2 ± 2.7	**
$CD8^+CD69^+$ (% of $CD3^+$)	1.00 ± 0.10	0.79 ± 0.06	1.18 ± 0.16	
$CD4^+IL\text{-}17^+$ (% of $CD4^+$)	0.49 ± 0.20	0.21 ± 0.11	0.43 ± 0.11	
$CD8^+IL\text{-}17^+$ (% of $CD8^+$)	0.01 ± 0.03	0.01 ± 0.01	0.02 ± 0.02	
gdT cell (% of $CD3^+$)	4.85 ± 0.58	4.32 ± 1.18	4.80 ± 0.86	
NKT cell (% of $CD3^+$)	1.43 ± 0.19	1.24 ± 0.19	1.57 ± 0.45	

M7 I.N. NALT				
CD4 (% of $CD3^+$)	48.3 ± 5.5	62.5 ± 5.6	42.2 ± 3.1	***
$CD4^+CD69^+$ (% of $CD3^+$)	7.6 ± 2.3	9.4 ± 1.4	5.7 ± 1.8	*p=0.07*
$CD8^+$ (% of $CD3^+$)	43.5 ± 4.35	28.2 ± 6.5	49.9 ± 3.2	***
$CD8^+CD69^+$ (% of $CD3^+$)	2.8 ± 1.9	3.54 ± 0.7	2.0 ± 0.3	
$CD4^+$IL-17^+ (% of $CD4^+$)	0.35 ± 0.45	0.18 ± 0.21	0.51 ± 0.69	
$CD8^+$IL-17^+ (% of $CD8^+$)	1.05 ± 1.85	1.11 ± 0.64	0.32 ± 0.42	
gdT cell (% of $CD3^+$)	2.87 ± 0.84	4.43 ± 1.8	1.89 ± 1.15	*
NKT cell (% of $CD3^+$)	1.22 ± 0.38	1.43 ± 0.11	2.02 ± 0.63	*
M7 I.N. Spleen				
CD4 (% of $CD3^+$)	54.4 ± 6.6	57.2 ± 3.6	48.3 ± 1.84	***
$CD4^+CD69^+$ (% of $CD3^+$)	3.2 ± 0.7	3.8 ± 0.5	3.5 ± 0.6	*p=0.06*
$CD8^+$ (% of $CD3^+$)	34.13 ± 6.2	29.3 ± 4.2	33.2 ± 2.0	***
$CD8^+CD69^+$ (% of $CD3^+$)	2.0 ± 0.3	2.7 ± 0.6	2.1 ± 0.4	
$CD4^+$IL-17^+ (% of $CD4^+$)	0.62 ± 0.16	0.47 ± 0.42	0.78 ± 0.31	
$CD8^+$IL-17^+ (% of $CD8^+$)	0.37 ± 0.25	0.96 ± 0.73	0.07 ± 0.04	
gdT cell (% of $CD3^+$)	2.49 ± 0.39	4.62 ± 1.44	2.25 ± 0.32	**
NKT cell (% of $CD3^+$)	2.56 ± 0.07	4.42 ± 1.06	3.29 ± 0.51	**

Supplementary References

1. Paul S, Sidney J, Sette A, Peters B. TepiTool: A Pipeline for Computational Prediction of T Cell Epitope Candidates. Curr Protoc Immunol. 2016;114:18 9 1- 9 24.